Supporting Information

for

Quantifying and Observing Viscoplasticity at the Nanoscale: Highly Localized Deformation Mechanisms in Ultrathin Nanocrystalline Gold Films

Ehsan Hosseinian, Marc Legros, and Olivier N. Pierron*

S1. Drift characterization of MEMS device

The relaxation experiments require proper stability of the MEMS setup to enable accurate calculation of the plastic strain and stress evolutions with time. The mechanical stability of the thermal actuator was checked by applying V_{in} = 3 V for 1 hour inside the TEM. No drift in the thermal actuator displacement X_A (without any specimen) could be detected by comparing TEM images. In addition, for ex situ experiments, no visible signs of thermal degradation was observed on the actuator surface after multiple device use at V_{in} = 3V for several days. The electrical stability of the MEMS setup was also characterized by monitoring the changes in ΔC_1 at a given V_{in} (when no specimen is attached) before and after long ex situ tests. Fig.S1 shows these changes for 4 different specimens, which vary between -3 and +1 fF (specimens 3 and 4, with lower amount of drifts, correspond to shorter tests). These changes suggest electrical drift, also evidenced when measuring the evolution of ΔC_1 as a function of time without any specimen. However, the measured total changes in ΔC_1- ΔC_2 during the relaxation experiments, also shown in Fig.S1, are at least 3 times more than the measured drift, and always positive values (consistent with relaxation). Therefore, while the occurrence of electrical drift during these tests cannot be ruled out, the measured signal for the relaxation experiments is most likely related to the viscoplastic deformation of the Au specimens. This is also confirmed in the stress-strain curves shown in Fig.4 and 5.

S2. Fabrication and characterization of free standing 100-nm thick Au films

The ultrathin freestanding Au specimens have been deposited on (100) Si substrates. First, high resolution photo-lithography was performed with a negative resist. This is the critical step to minimize the line edge roughness of the specimens. To remove any residues from the previous steps and remove the native oxide, the patterned die was exposed to 90-second descum in a Vision Reactive Ion Etching (RIE) tool. Au films with thicknesses of 100 nm were deposited using a Denton Ebeam Evaporator with a base pressure of 8×10^{-7} Torr and a rate of 0.5 Å/sec with 99.99% purity of the target. The deposition was interrupted for 15 min after depositing half of the final thickness to minimize the growth of columnar grains. Then, a lift-off technique was used by acoustic agitation in an acetone solution. Finally, the specimens were released from the Si substrate by XeF_2 etching of Si (using a Xactix XeF_2 etcher).

Au specimens were fabricated with gauge lengths of 20 μm and with gauge widths of 1.5 μm. While the length of the samples were very precise, the gage width varied slightly depending on process conditions. The thickness of the thin film specimens, fabricated by Denton evaporator, is highly uniform with a variation of less than ~5 nm. The grain structure of the samples was characterized in a F30 Technai transmission electron microscope. Figure S1 shows TEM images of the NC gold (Au) thin film specimens with thickness of 100 nm. These images show a NC microstructure with a wide distribution of grain size ranging from 20 to 300 nm. Selected area electron diffraction patterns in inset of Figure S2(a) reveal a heterogeneous microstructure without any strong out-of-plane or in-plane texture. The lack of a strong (111) out-of-plane texture, typically observed for thin Au films, may result from the deposition of the film on a Si substrate with the presence of a thin native oxide.

S3. Equations for grain-boundary-diffusion-based mechanisms

The grain boundary sliding (GBS) mechanism controlled by grain boundary diffusion is governed by the following equation:

$$\dot{\varepsilon} = 2\times10^{5} D_{0,gb} \exp\left(\frac{-Q_{gb}}{RT}\right)\frac{\mu b}{kT}\left(\frac{b}{d}\right)^{3}\left(\frac{\sigma}{\mu}\right)^{2} \quad \text{(S1)}$$

where $D_{0,\mathrm{gb}}$ is the pre-exponential coefficient for grain boundary diffusion, Q_{gb} is the activation energy for grain boundary diffusion, k is Boltzmann's constant, T is the absolute temperature (T = 300 K), μ is the shear modulus, b is Burger's vector, d is the average grain size, and σ is the applied stress. The Coble creep equation is given by:

$$\dot{\varepsilon} = 14\pi\delta D_{0,gb} \exp\left(\frac{-Q_{gb}}{RT}\right)\frac{\Omega}{RT}\frac{\sigma}{d^{3}} \quad \text{(S2)}$$

where δ is the grain boundary width, Ω is the molar volume, and R is the ideal gas constant. Finally, the Asbhy-Verral mechanism is governed by the following equation:

$$\dot{\varepsilon} = 330\delta D_{0,gb} \exp\left(\frac{-Q_{gb}}{RT}\right)\frac{\Omega}{RT}\left(\frac{\sigma}{d^{3}} - \frac{0.72\Gamma}{d^{4}}\right) \quad \text{(S3)}$$

where Γ is the grain boundary free energy. Table S1 lists the values of all the material parameters for nanocrystalline Au.[1]

$D_{0,\mathrm{gb}}$ (m^2/s)	Q_{gb} (kJ/mol)	μ (GPa)	b (nm)	d (nm)	δ (nm)	Ω (m^3/mol)	Γ (J/m^2)
6.2×10^{-7}	85	25	0.282	75	0.5	1.44×10^{-5}	0.2

Table S1. Material parameters for nanocrystalline Au

S4. Image-based stress and strain calculations

The electronic sensing was not operational during the in situ TEM tests which were performed inside a JEOL microscope. Hence an indirect approach was used to estimate stress and strain. Fig.S4(a) shows a selection of bright field TEM images that were used to measure the displacements of the load sensor (based on the displacement of the capacitive sensor 2) for selected V_{in} values. The displacements are measured by comparing the images at a given V_{in} to the reference image at V_{in} = 0V. The features of interest were a fixed comb, an adjacent moving comb of CS2, and the gap in between. A MATLAB routine was created to measure the gaps from these images, from which the displacement of load sensor (X_{LS}) can be obtained. In addition, the specimen elongation (X_S) was directly measured using bright field TEM images of the gauge section at magnifications of 10 or 12K, with a resolution of ~30 nm (see Fig.S4(b)).

S5. Grain orientation for in situ TEM experiments

Fig.S5 represents the stereographic projection corresponding to grains G1 and G2 in Fig.8. The sheared grain boundary corresponds to the (111) plane of G2 and the (-1-1-1) plane in G1 (bold line in Fig.S5). The markers X and Y in Fig.8 are probably stacking faults or nanotwins oriented along (-1-11) in G2. They remain immobile and mostly unaffected by the plastic deformation that occurs along the G1/G2 interface, which make them relevant to serve as markers for local strain measurement. Fig 9a and 9b, taken 45minutes apart with the same imaging conditions, show that despite the large strain experienced at the G1 and G2 interface, X2 and Y2 did not change neither in direction or width. The apparent change in contrast observed on these markers in Fig S6 is due to a slight tilt of the TEM straining holder during the experiment, a common maneuver, frequently repeated to adjust the contrast of a deforming sample. The direction of the tensile axis is vertical in Figures 8, 9 and S6.

Fig.S7 represents the stereographic projection corresponding to the grain sheared by intragranular dislocations along the (-1-1-1) plane in Fig.9. Note that in both cases (Fig.8 and 9, the localized shear occurs along a plane close to the maximum shear with respect to the tensile axis. In Fig. 9, the most probable Burgers vector a/2{-101} leads to a Schmid factor of 0.44.

References

1. G. D. Sim and J. J. Vlassak, *Scripta Materialia*, 2014, **75**, 34-37.

Supporting Figures

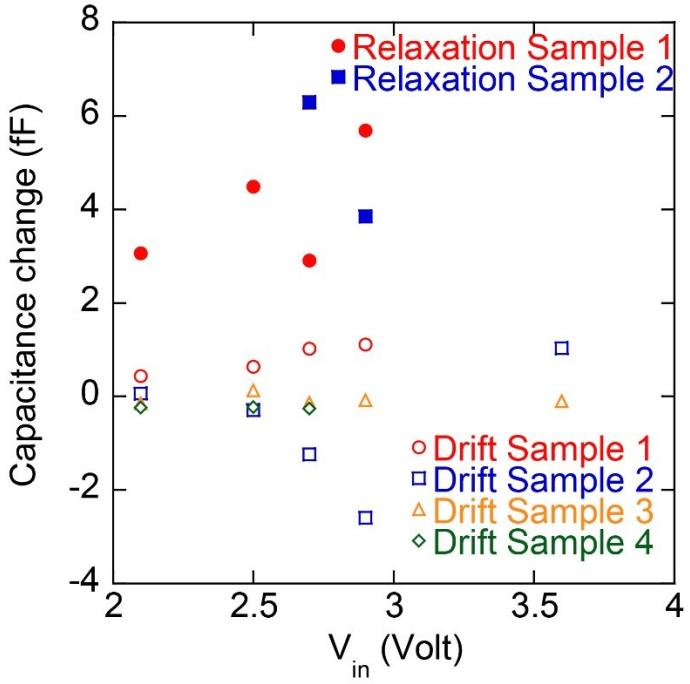

Fig.S1 Comparison of ΔCS measurements for the MEMS setup for the relaxation tests (MEMS with specimen) and drift experiments (MEMS without any specimen) in different applied V_{in}.

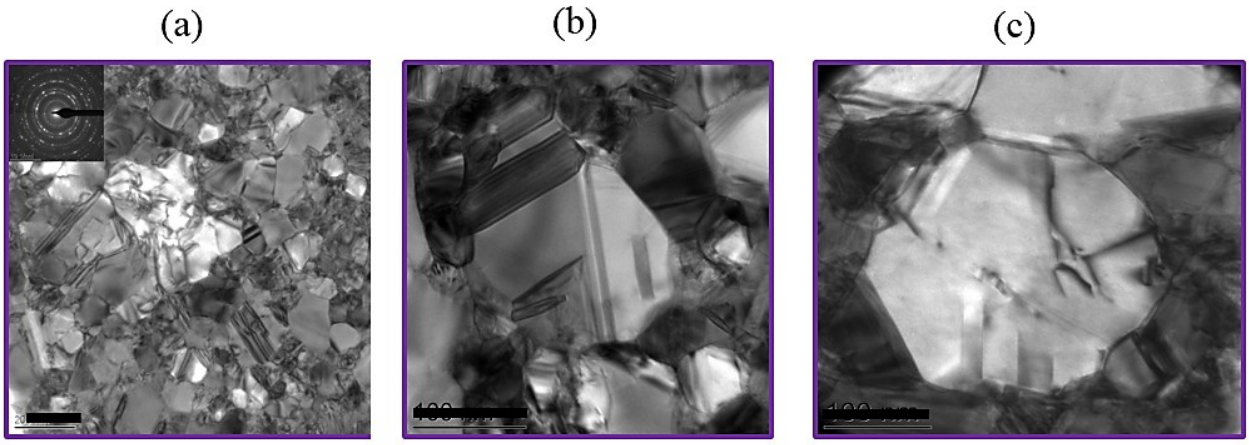

Fig. S2 Bright field TEM images of the free standing Au specimens showing: (a) nanocrystalline structure of the film with no planar texture according to SAED pattern in the inset (scale bar is 200 nm); (b) An ultrafine grain with twin and stacking faults (scale bar is 100 nm); (c) a grain with two stacking faults and dislocation (scale bars is 100 nm).

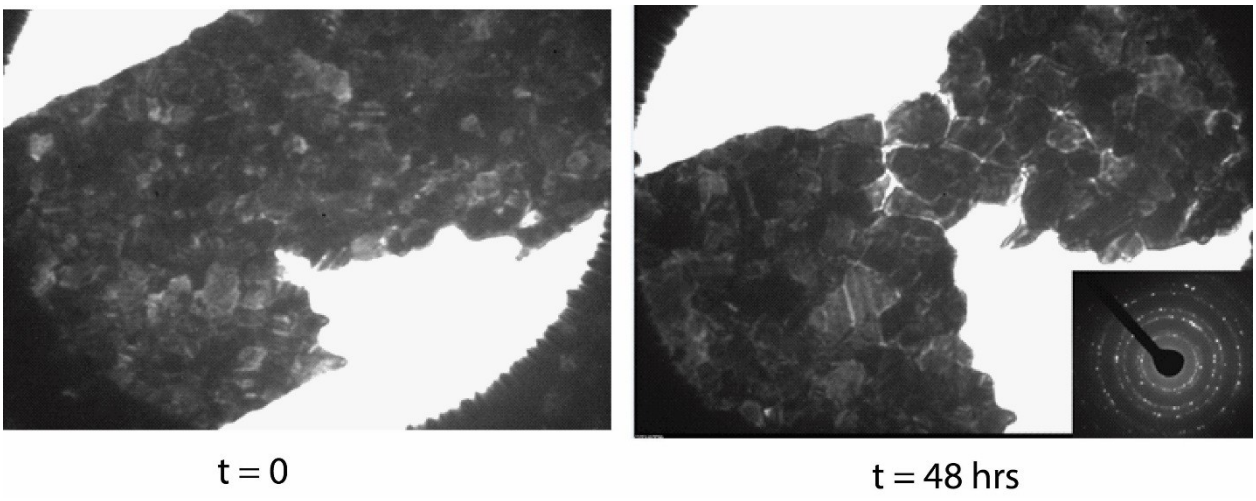

Fig.S3 Evolution of microstructure and crack advance ahead of a pre-existing defect for a 2-day-long stress relaxation experiment performed inside the TEM. Numerous voids along the grain boundaries can be observed at t = 48 hours

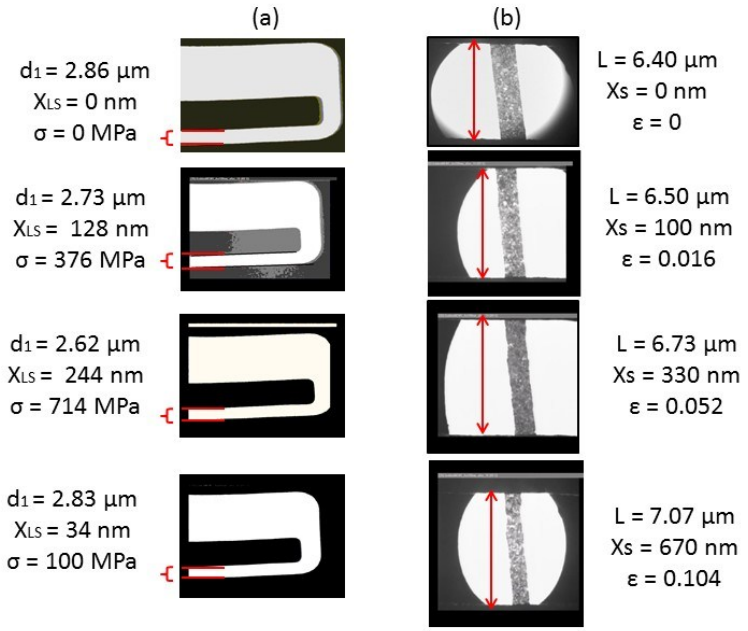

Fig.S4 (a) Series of TEM images of capacitive sensor 2 during a relaxation test (specimen 2, see main manuscript), at four different V_{in} values (0, 1.8, 2, and 2.4 V), to measure stress. (b) Corresponding TEM images of gauge length to measure strain.

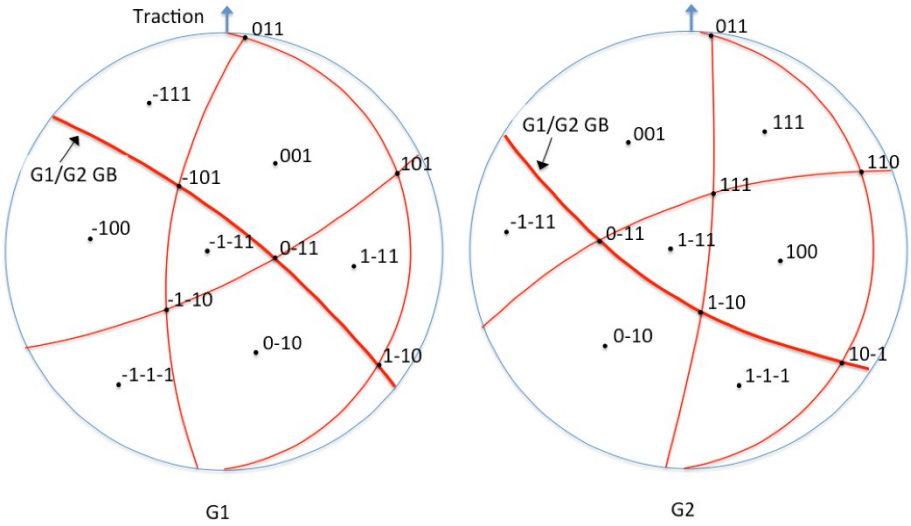

Fig.S5 Stereographic projections of G1 and G2 grains in Fig.8.

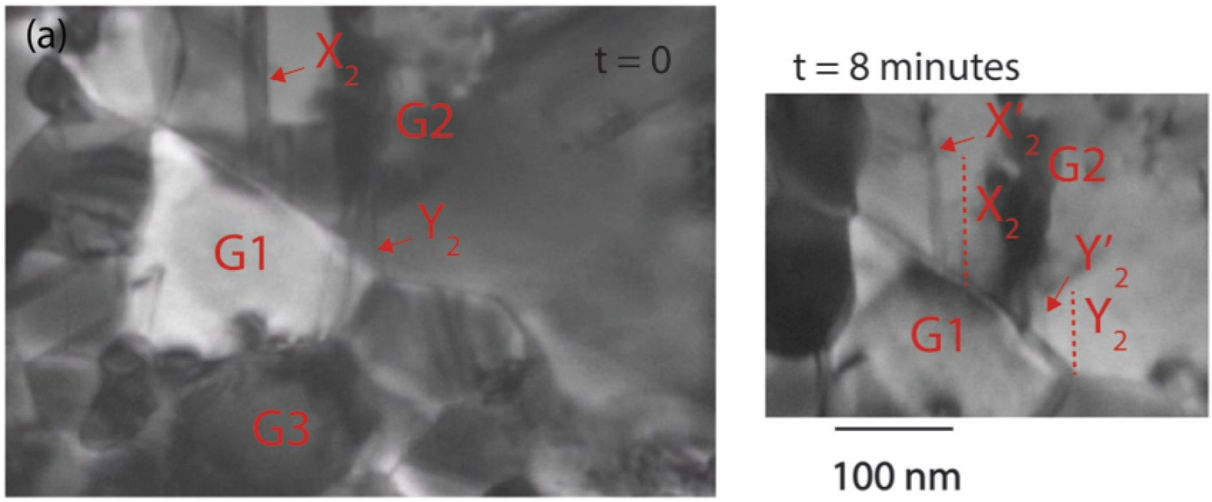

Fig.S6 Intergranular shear between grains G1 and G2 after 8 min relaxation. The shear measured along the G1/G2 interface is 30 nm. X_2 and Y_2 are fixed markers (immobile stacking faults in grain G2).

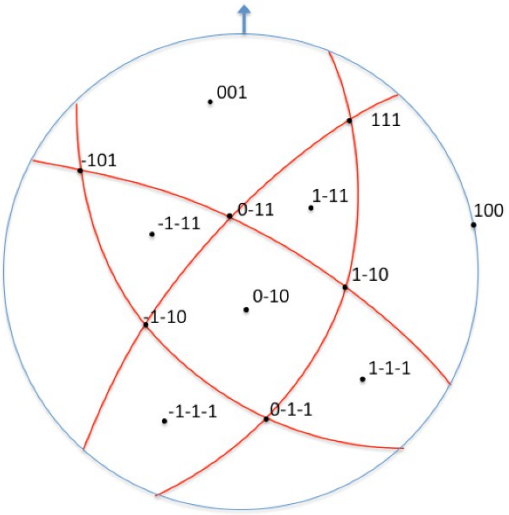

Fig.S7 Stereographic projection of the grain sheared by intragranular dislocations in Fig.9.